Molecular Pharmacology Fast Forward. Published on January 14, 2013 as DOI: 10.1124/mol.112.084384
Molecular Pharmacology Fast Forward. Published on January 14, 2013 as doi:10.1124/mol.112.084384
This article has not been copyedited and formatted. The final version may differ from this version.

ICA-105574 interacts with a common binding site to elicit opposite effects on inactivation gating of EAG and ERG potassium channels

Vivek Garg, Anna Stary-Weinzinger and Michael C. Sanguinetti

Nora Eccles Harrison Cardiovascular Research & Training Institute, Department of Physiology, Department of Medicine University of Utah, Salt Lake City (V.G., M.C.S.), and Department of Pharmacology and Toxicology, University of Vienna, Vienna, Austria (A. S.-W.)

Downloaded from molpharm.aspetjournals.org at ASPET Journals on April 17, 2024

Copyright 2013 by the American Society for Pharmacology and Experimental Therapeutics.

Molecular Pharmacology Fast Forward. Published on January 14, 2013 as DOI: 10.1124/mol.112.084384
This article has not been copyedited and formatted. The final version may differ from this version.

Running title: Activator binding site on *ether-a-go-go* K^+ channels

Corresponding author:

Michael C. Sanguinetti

Nora Eccles Harrison Cardiovascular Research & Training Institute

University of Utah

95 South 2000 East

Salt Lake City, UT 84112

tele: 801-581-3058

fax: 801-581-3128

Email: sanguinetti@cvrti.utah.edu

32 pages
1 table
6 figures

# of words in the *Abstract*: 238

# of words in the *Introduction*: 538

# of words in the *Discussion*: 1056

Supporting Information: 5 Figures (Figs. S1– S5)

ABBREVIATIONS:

bEAG1, bovine *ether-a-go-go* type 1; hEAG1, human *ether-a-go-go* type 1*;* hERG1, human *ether-a-go-go-related* gene type 1; ICA, 3-nitro-N-(4-phenoxyphenyl)-benzamide (ICA-105574); I_{Kr}, rapid delayed rectifier K^+ current; I_{end}, current at the end of the pulse, I_{peak}, peak outward current

Downloaded from molpharm.aspetjournals.org at ASPET Journals on April 17, 2024

Molecular Pharmacology Fast Forward. Published on January 14, 2013 as DOI: 10.1124/mol.112.084384
This article has not been copyedited and formatted. The final version may differ from this version.

ABSTRACT

Rapid and voltage-dependent inactivation greatly attenuates outward currents in *ether-a-go-go-related* gene (ERG) K^+ channels. In contrast, inactivation of related *ether-a-go-go* (EAG) K^+ channels is very slow and minimally reduces outward currents. ICA-105574 (ICA, or 3-nitro-N-(4-phenoxyphenyl)-benzamide) has opposite effects on inactivation of these two channel types. Whereas ICA greatly attenuates ERG inactivation by shifting its voltage-dependence to more positive potentials, it enhances the rate and extent of EAG inactivation without altering its voltage dependence. Here we investigate whether the inverse functional response to ICA in EAG and ERG channels is related to differences in ICA binding site or intrinsic mechanisms of inactivation. Molecular modeling coupled with site-directed mutagenesis suggests that ICA binds in a channel-specific orientation to a hydrophobic pocket bounded by the S5/pore helix/S6 of one subunit and S6 of an adjacent subunit. ICA is a mixed agonist of mutant EAG and EAG/ERG chimera channels that inactivate by a combination of slow and fast mechanisms. With the exception of three residues, the specific amino acids that form the putative binding pocket for ICA in ERG are conserved in EAG. Mutations introduced into EAG to replicate the ICA binding site in ERG did not alter the functional response to ICA. Together these findings suggest that ICA binds to the same site in EAG and ERG channels to elicit opposite functional effects. The resultant agonist or antagonist activity is determined solely by channel-specific differences in the mechanisms of inactivation gating.

Downloaded from molpharm.aspetjournals.org at ASPET Journals on April 17, 2024

Molecular Pharmacology Fast Forward. Published on January 14, 2013 as DOI: 10.1124/mol.112.084384
This article has not been copyedited and formatted. The final version may differ from this version.

Introduction

Ether-a-go-go (EAG) K^+ channels, first described in *Drosophila* (Warmke et al., 1991), are highly expressed in the mammalian CNS (Ludwig et al., 1994; Martin et al., 2008) and a variety of tumors (Hemmerlein et al., 2006; Mello de Queiroz et al., 2006; Pardo et al., 1999). EAG channels activate rapidly and exhibit only a very subtle and slow form of inactivation (Garg et al., 2012). The related *ether-a-go-go-related gene* (ERG) K^+ channel was discovered by screening of a human hippocampus cDNA library (Warmke and Ganetzky, 1994) and functional analysis revealed that it activates more slowly than EAG and undergoes a very rapid inactivation that greatly reduces channel open probability at positive potentials (Smith et al., 1996; Spector et al., 1996). Both slow (EAG) and fast (ERG) inactivation are proposed to be mediated by structural rearrangement of the selectivity filter (Garg et al., 2012; Stansfeld et al., 2008) that is commonly referred to as C- or P/C-type inactivation (Chen et al., 2000; Hoshi et al., 1991) to differentiate it from the well characterized N-type inactivation of Kv channels (Hoshi et al., 1990).

In the human heart, ERG type 1 (hERG1, Kv11.1) channels conduct the rapid delayed rectifier K^+ current, I_{Kr} (Sanguinetti et al., 1995; Sanguinetti and Jurkiewicz, 1990; Trudeau et al., 1995). Rapid inactivation of I_{Kr} during the plateau phase of the action potential delays repolarization and facilitates Ca^{2+} entry into the cardiomyocyte that triggers excitation-contraction coupling. Pathological reduction of I_{Kr} caused either by congenital mutations in hERG1 or block of channels as a side effect of many common medications is associated with a prolonged QT interval and an increased risk of cardiac arrhythmia (Sanguinetti and Tristani-Firouzi, 2006). This potentially life-threatening side-effect prompted the now routine screening of hERG1 channel activity of compounds during the early phase of drug development programs.

Downloaded from molpharm.aspetjournals.org at ASPET Journals on April 17, 2024

Molecular Pharmacology Fast Forward. Published on January 14, 2013 as DOI: 10.1124/mol.112.084384
This article has not been copyedited and formatted. The final version may differ from this version.

An unanticipated outcome of these routine screens was the discovery of compounds that activate, rather than block, hERG1 channels. Activators of hERG1 could theoretically be used to treat or prevent arrhythmia associated with congenital long QT syndrome (Zhang et al., 2012).

3-Nitro-N-(4-phenoxyphenyl)-benzamide (ICA-105574, or ICA) is a recently discovered compound that shortens the duration of cardiac action potentials by inducing a dramatic shift in the voltage dependence of hERG1 inactivation to more positive potentials (e.g., +183 mV at 2 μM) (Gerlach et al., 2010). In striking contrast to its inhibition of hERG1 channel inactivation, we recently reported that ICA enhances inactivation of human EAG1 (hEAG1, Kv10.1) channels (Garg et al., 2012). In addition to differences in their response to ICA, inactivation of hERG1, but not hEAG1, is slowed by external tetraethylammonium and elevated $[K^+]_e$ (Garg et al., 2012). Despite these differences, the selectivity filter appears to serve as the inactivation gate in both hERG1 and hEAG1 channels (Garg et al., 2012; Smith et al., 1996). The disparate effects of ICA on intrinsic inactivation of such closely related Kv channels could result from ligand binding to distinct sites on the two channels or reflect inverse modulation of distinct, channel-specific modes of inactivation. Here we use molecular modeling and analysis of mutant hEAG1 and bovine EAG1/hERG1 chimera channels to explore whether the ICA binding site in hEAG1 is homologous to the site previously reported for hERG1 (Garg et al., 2011).

Downloaded from molpharm.aspetjournals.org at ASPET Journals on April 17, 2024

Materials and Methods

Molecular biology. Human *EAG1* (*KCNH1*; NCBI Reference Sequence: NM_002238.3) cDNA cloned into psGEMHE oocyte expression vector was kindly provided by the late Dr. Dennis Wray. *HERG1* (*KCNH2*, isoform 1a, NCBI Reference Sequence: NM_000238.2) (24), was cloned into the pSP64 oocyte expression vector. Mutations in WT *hEAG1* cDNA were made

Molecular Pharmacology Fast Forward. Published on January 14, 2013 as DOI: 10.1124/mol.112.084384
This article has not been copyedited and formatted. The final version may differ from this version.

using the QuikChange site-directed mutagenesis kit (Agilent Technologies, Santa Clara, CA) and verified by DNA sequence analyses. Plasmids were linearized by NotI (psGEMHE) or EcoR1 (pSP64). *HEAG1* cRNA was in vitro transcribed with the mMessage mMachine T7 kit (Life Technologies, Grand Island, NY). *HERG1* cRNA was prepared with the mMessage mMachine SP6 kit (Ambion, Austin, TX). [cRNA] was quantified by RiboGreen assay (Life Technologies).

Two-electrode voltage clamp of *Xenopus* oocytes. Procedures for harvesting oocytes from *Xenopus laevis* was as described (Garg et al., 2012) and was approved by the University of Utah Institutional Animal Care and Use Committee. The isolation, culture, and injection of oocytes with cRNA were performed as described (Goldin, 1991; Stühmer, 1992). Injected oocytes were incubated for 1-5 days at 18°C in Barth's saline solution before use in voltage clamp experiments. Currents were recorded from oocytes using a standard two-microelectrode voltage clamp technique (Goldin, 1991; Stühmer, 1992) and agarose-cushion microelectrodes (Schreibmayer et al., 1994). A GeneClamp 500 amplifier, Digidata 1322A data acquisition system, and pCLAMP 9.0 software (Molecular Devices, Inc., Sunnyvale, CA) were used to produce command voltages and to record current and voltage signals.

Oocytes were bathed in KCM211 solution at room temperature (22–24°C). To record ionic currents, the oocyte was voltage clamped to a holding potential (V_h) of −100 mV, and 1-s pulses were applied to a test potential (V_t) of 0 mV every 10 s until current magnitude reached a steady-state level. During perfusion of the recording chamber with ICA solutions, the pulse interval was lengthened to 30 s. After currents achieved a new steady-state level in the presence of ICA, *I-V* relationships were determined if needed.

Solutions. Barth's solution contained (in mM): 88 NaCl, 2 KCl, 0.41 $CaCl_2$, 0.33 $Ca(NO_3)_2$, 1 $MgSO_4$, 2.4 $NaHCO_3$, 10 HEPES, 1 pyruvate, 50 mg/L gentamycin; pH was

Downloaded from molpharm.aspetjournals.org at ASPET Journals on April 17, 2024

Molecular Pharmacology Fast Forward. Published on January 14, 2013 as DOI: 10.1124/mol.112.084384
This article has not been copyedited and formatted. The final version may differ from this version.

adjusted to 7.4 with NaOH. KCM211 solution contained (in mM): 98 NaCl, 2 KCl, 1 $CaCl_2$, 1 $MgCl_2$, 5 HEPES; pH was adjusted to 7.6 with NaOH. ICA was purchased from Sigma-Aldrich (St. Louis, MO) and AKos GmBH (Steinen, Germany) and prepared as a 10 mM stock solution in dimethyl sulfoxide. Final [ICA] was obtained by dilution of the stock solution with KCM211 immediately before use for each experiment. TEA was purchased from Sigma-Aldrich.

Data analysis. Digitized data was analyzed off-line with pCLAMP9 (Molecular Devices), ORIGIN 8 (OriginLab, Northhampton, MA) and Excel (Microsoft Corp., Redmond, WA) software. The concentration–effect relationship for ICA inhibition of hEAG current measured at +30 mV was fitted with a Hill equation. ICA enhanced currents at low concentrations and reduced currents at high concentrations of some mutant channels. For these mutant channels, an effective IC_{50} (indicated in Table 1) was determined simply by noting the concentration that reduced control current by 50%. All data are expressed as mean ± SEM (n = number of oocytes) and evaluated by an unpaired Student's t-test where appropriate ($p \leq 0.05$ was considered a statistically significant difference).

Molecular Modeling. Homology models of the closed and open channel conformations were generated with Modeller9v9 using the KcsA crystal structure (pdb ID: 2HVK) for the closed and the KvAP (1ORQ) and the high resolution Mthk (pdb ID: 3LDC) crystal structures as templates for the open conformation. Modeling details were described previously (Stary et al., 2010).

All mutant hEAG1 channels (F359L, M431F/M458L/L463M) were generated in Pymol. MD simulations of open and closed models were performed with Gromacs v.4.5.4 (Hess et al., 2008). WT and mutant channels were embedded in an equilibrated simulation box consisting of 280 dioleolylphosphatidylcholine (DOPC) lipids. Lipid parameters were taken from Siu, et al.

Downloaded from molpharm.aspetjournals.org at ASPET Journals on April 17, 2024

Molecular Pharmacology Fast Forward. Published on January 14, 2013 as DOI: 10.1124/mol.112.084384
This article has not been copyedited and formatted. The final version may differ from this version.

(Siu et al., 2008) and the TIP3P water model was utilized (Jorgensen et al., 1983). The amber99sb force field (Hornak et al., 2006) was used for the protein. Electrostatic interactions were calculated explicitly at a distance <1 nm, long-range electrostatic interactions were calculated at every step by particle-mesh Ewald summation (Darden et al., 1993). Lennard–Jones interactions were calculated with a cutoff of 1 nm. All bonds were constrained by using the LINCS algorithm (Hess et al., 1997), allowing for an integration time step of 2 fs. The Nose-Hoover thermostat (Nose, 1984) was used for temperature coupling (τ = 0.1 ps) and the Parrinello-Rahman barostat algorithm (Parrinello and Rahman, 1981) for pressure coupling. 1000 conjugate gradient energy-minimization steps were performed, followed by 2 ns of restrained MD in which the protein atoms were restrained with a force constant of 1000kJ/mol^{-1}nm^{-2} to their initial position, while ions, lipids and solvent were allowed to move freely. Each system was then subjected to 50 ns of unrestrained MD, during which coordinates were saved every 10 ps for analysis.

Coordinates of ICA were generated with Gaussview 5 and the geometry optimized with the Hartee-Fock 3-21G basis set implemented in Gaussian09 (Frisch et al., 2009). Docking was performed with the program Gold 4.0.1 (Jones et al., 1995). Coordinates of the geometric center calculated among residues F359, L434, M431, Y464 and F468 were taken as binding site origin. The binding site radius was set equal to 10 Å. 150,000 operations of the GOLD genetic algorithm were used to dock the selected compounds into the WT and mutant channels. 3 snapshots (15 ns, 33 ns, 50 ns) were taken from MD trajectories. The stability of the predicted binding modes of ICA to WT hEAG1 channels in open and closed conformation was confirmed in 50 ns MD simulations as described previously (Knape et al., 2011).

Downloaded from molpharm.aspetjournals.org at ASPET Journals on April 17, 2024

Molecular Pharmacology Fast Forward. Published on January 14, 2013 as DOI: 10.1124/mol.112.084384
This article has not been copyedited and formatted. The final version may differ from this version.

Results

ICA Binds to the Pore Domain of hERG1 and hEAG1 Channels to Exert Opposite Effects on Inactivation.

The effects of ICA on wild-type (WT) hERG1 and hEAG1 channels expressed in *Xenopus* oocytes are illustrated in Fig. 1. Channels were activated with a 10-s pulse to +30 mV from a holding potential of −100 mV. As reported previously (Garg et al., 2012; Garg et al., 2011; Gerlach et al., 2010), ICA caused a marked and concentration-dependent enhancement of hERG1 current (Fig. 1*A*), but an inhibition of hEAG1 current (Fig. 1*B*) by reducing both the initial peak outward current (I_{peak}) and inducing a time-dependent decay of current during the pulse. Inhibition of hEAG1 current by ICA is caused by an enhancement of intrinsic inactivation and is not due to open channel block (Garg et al., 2012). The inhibitory effect of ICA on hEAG1 was more potent than the activation effect on hERG1 channels. The IC_{50} for ICA inhibition of hEAG1 was 1.38 ± 0.04 μM for I_{peak} and 0.44 ± 0.03 μM for current at the end of the pulse, I_{end} (n = 5), current measured at the end of the pulse (Fig. 1*C*).

Using scanning mutagenesis and functional analysis of mutant hERG1 channels, we recently proposed that ICA binds to a hydrophobic pocket formed by the S5/pore helix/S6 of one subunit and S6 segment of an adjacent channel subunit (Garg et al., 2011). To identify the region of the EAG1 channel responsible for the inhibitory effect of ICA, we first used an unbiased approach and examined several previously characterized chimera channels (Ficker et al., 1998) constructed from bovine EAG1 (bEAG1) and hERG1. The amino acid sequences of bovine and human EAG1 are 97% identical for the entire proteins and 100% identical in the S1-S6 regions. First, the role of the pore module was investigated. ICA was an agonist when the pore region (S45 linker-S6) of the chimera channel was contributed by hERG1 (Fig. 1*D*), but was an antagonist when the same pore region was supplied by bEAG1 (Fig. 1*E*). Next, ICA was tested on chimeras

Downloaded from molpharm.aspetjournals.org at ASPET Journals on April 17, 2024

Molecular Pharmacology Fast Forward. Published on January 14, 2013 as DOI: 10.1124/mol.112.084384
This article has not been copyedited and formatted. The final version may differ from this version.

in which only a limited region of the pore domain of hERG1 was replaced by their bEAG1 counterpart. When only the S6 segment (Fig. 1*F*) or the turret (Fig. 1*G*) was supplied by bEAG1, ICA acted as an agonist. Finally, when the S45 linker-S5 (Fig. 1*H*) or the turret-pore helix-selectivity filter (Fig. 1*I*) was supplied by bEAG1, the effects of ICA were biphasic; 30 μM ICA induced or enhanced the rate of slow inactivation and caused a smaller increase in current compared to 10 μM ICA. Together the findings obtained with hERG1/bEAG1 chimeras indicate that the pore domain (S5-S6) region determines the channel-specific response to ICA.

ICA is a Mixed Agonist of a Fast-Inactivating Mutant hEAG1 Channel. Two Ser residues, located on either side of the selectivity filter, are key determinants of fast P/C-type inactivation in hERG1 (Suessbrich et al., 1997). In bEAG1 channels, combined mutation of the residues located in the homologous position as these two Serines induces fast inactivation (Ficker et al., 1998). Introduction of the same two mutations (T432S/A443S) into hEAG1 also induces a rapid, time-dependent decay of outward current (Fig. 2*A*), and similar to P/C-type inactivation of hERG1 (Smith et al., 1996), its rate is slowed by extracellular tetraethylammonium (TEA, 10 mM) or elevated $[K^+]_e$ (Supplemental Fig. 1). In contrast, the rate of the comparatively very slow inactivation of hEAG1 is unaffected by TEA or changes in $[K^+]_e$ (Garg et al., 2012). When activated by a 0.4 s pulse to +30 mV, 3 μM ICA reduced I_{peak} and the inactivating component of outward T432S/A443S hEAG1 current, but doubled the magnitude of I_{end} (Fig. 2*A*). At 30 μM, ICA eliminated fast inactivation (Fig. 2*A*). ICA (1 - 30 μM) reduced I_{peak} in a concentration-dependent manner (Fig. 2*B*), but exhibited a biphasic (mixed agonist) effect on I_{end} and reduced rectification of the I_{end} -V relationship (Fig. 2*C*). At 30 μM, ICA inhibited I_{peak} (all potentials) and I_{end} (at test potentials < +10 mV). The [ICA]-response relationship for I_{peak} and I_{end} at a single voltage (+30 mV) for T432S/A443S hEAG1 channels is

Downloaded from molpharm.aspetjournals.org at ASPET Journals on April 17, 2024

Molecular Pharmacology Fast Forward. Published on January 14, 2013 as DOI: 10.1124/mol.112.084384
This article has not been copyedited and formatted. The final version may differ from this version.

compared to WT channels in Fig. 2*D*. Together, these findings suggest that the multiple effects of ICA on T432S/A443S hEAG1 channels represent the sum of two opposing actions: reduced fast (ERG1-like) inactivation to increase current plus inhibition, perhaps mediated by open channel block to reduce current. We next explore whether the opposite effects of ICA on fast versus slow modes of inactivation gating are mediated by ICA binding to the same or distinct sites in hERG1 and hEAG1 channels.

Molecular Determinants of ICA Interaction with hEAG1 Channels. Simulated docking of ICA to molecular models of the hEAG1 pore module was performed and the findings compared to our previous model of ICA bound to the hERG1 channel. Homology models of hEAG1 were constructed using the KvAP and MthK crystal structures (Jiang et al., 2003; Ye et al., 2003) as template for the open state and the KcsA crystal structure (Doyle et al., 1998) as template for the closed state. In hERG1, ICA was predicted to be oriented perpendicular to the axis of the S5 and S6 segments in both the closed and open state dockings, with the nitro group facing towards the pore (Garg et al., 2011). For hEAG1, ICA also favored a perpendicular orientation in the open state, but the nitro group faces away from the pore and towards the lipids that surround the pore module (Fig. 3*A*-*C*). In the closed state of hEAG1, ICA is orientated parallel to S5 and S6 (Fig. 3*D*-*F*). Simulated docking of ICA to the open states of hERG1 and hEAG1 are compared in Supplemental Fig. 2. In hEAG1, ICA resides in a hydrophobic pocket formed by residues Met431, Leu434, Met458, Tyr464, Ile467 and Phe359. The location of this binding pocket is quite similar to that previously described for hERG1 (Garg et al., 2011). However, sequence differences between hERG1 and hEAG1 lead to different shaped binding pockets for ICA (Supplemental Figs. 2C, 2E). ICA protrudes deeply into the cleft between two adjacent subunits in the hERG1 channel (Supplemental Fig. 2A). By contrast, in hEAG1 Tyr464

Downloaded from molpharm.aspetjournals.org at ASPET Journals on April 17, 2024

Molecular Pharmacology Fast Forward. Published on January 14, 2013 as DOI: 10.1124/mol.112.084384
This article has not been copyedited and formatted. The final version may differ from this version.

forms a barrier at the S6-S6 interface, leading to a shallower binding mode for ICA (Fig. 3 and Supplemental Fig. 2D). ICA does not form π-π stacking interactions with Tyr464 in either the closed or open state of hEAG1 and thus, might not be able to stabilize the phenyl group in the down conformation as previously suggested for hERG1 (Garg et al., 2011). In addition, stabilizing hydrogen bonds predicted between ICA and selectivity filter residues in hERG1 are lacking in hEAG1.

Considering both open and closed hEAG1 model simulations, eleven residues are predicted to be in close proximity to ICA: Leu427, Met431 and Leu434 in the pore helix, Val356 and Phe359 in S5, and Leu463, Tyr464, Ile467, Phe468 in S6 of one subunit, plus Met457 and Met458 in the S6 of an adjacent subunit. To corroborate the modeling results, we mutated to Ala each of these 11 residues. Seven of the 11 Ala substitutions reduced the sensitivity (increased IC_{50}) of the mutant channel to ICA by >4-fold compared to WT hEAG1 (Table 1 and Supplemental Fig. 3). The I467A mutation increased the IC_{50} by 2.5-fold, while V356A, L427A and Y464A mutations reduced IC_{50} by 2.5 - 6-fold. Val356, Leu427 and Ile467 are predicted to interact with ICA in the closed, but not the open state. Because of the poor expression of L427A mutant channel (requiring 100 times more cRNA and longer incubation time in comparison to WT hEAG), and its location near the selectivity filter (P/C-type inactivation gate), Leu427 residue was not analyzed any further. To explore the potential significance of Ile467 and Val356 to ICA binding, each was mutated to the more perturbing Glu. Accordingly, both V356E and I467E mutations increased the IC_{50} for ICA by >55 fold (Table 1, Supplemental Fig. 3). Thus, mutagenesis confirmed the importance of all the residues predicted by molecular modeling to interact with ICA in either the open or closed state of the hEAG1 channel.

Some of the molecular determinants of ICA binding to hEAG1 align with those previously

Downloaded from molpharm.aspetjournals.org at ASPET Journals on April 17, 2024

Molecular Pharmacology Fast Forward. Published on January 14, 2013 as DOI: 10.1124/mol.112.084384
This article has not been copyedited and formatted. The final version may differ from this version.

described for hERG1. For example, mutation of Phe557, Phe619, Leu622 and Phe656 in hERG1 reduced the sensitivity to the activator effect of ICA (Garg et al., 2011); similarly, mutation of the corresponding residues to Ala in hEAG1 (Phe359, Met431, Leu434 and Phe468) reduced the inhibitory action of ICA. However, many homologous mutations yielded incongruous findings for the two channels. First and foremost, the Y652A hERG1 channel is nearly insensitive to activation by ICA (Garg et al., 2011), whereas the homologous Y464A hEAG1 channel is more sensitive to inhibition (more inactivated) by ICA (Garg et al., 2012). Second, while the mutations L463A and M458A decreased the sensitivity of hEAG1 channels (IC_{50} increased by 94-fold and 46-fold, respectively; Table 1) and V356A enhanced sensitivity to ICA ~6-fold, the corresponding mutations in hERG1 (M651A, L646A and M554A) were previously reported to not alter the response to ICA (Garg et al., 2011). Third, F557L hERG1 channels are insensitive to ICA, whereas the corresponding F359L hEAG1 channel is activated by ICA (Garg et al., 2012). We investigated these notable differences by further examining three of these key residues in hEAG1: Met458 and Tyr464 in S6 and Phe359 in S5.

Simulated dockings predicted that both Met458 in hEAG1 and the homologous residue Leu646 in hERG1 are in close proximity to ICA. Nonetheless, substitution of Leu646 to either Ala (Garg et al., 2011) or Glu (Supplemental Fig. 4) did not alter hERG1 channel sensitivity to ICA. As noted above, M458A mutation in hEAG1 reduced ICA sensitivity; however, similar to L646E in hERG1, M458E did not alter hEAG1 sensitivity to ICA (Table 1, Supplemental Fig. 4), presumably because the acidic side chain of Glu is repelled from the hydrophobic pocket and thus, does not affect ICA binding. In hERG1, three specific point mutations, Y652A (S6), F557L (S5) and L434C (pore helix), rendered the channel insensitive to 30 μM ICA, consistent with molecular modeling predictions (Garg et al., 2011). The effect of multiple ICA concentrations on

Downloaded from molpharm.aspetjournals.org at ASPET Journals on April 17, 2024

Molecular Pharmacology Fast Forward. Published on January 14, 2013 as DOI: 10.1124/mol.112.084384
This article has not been copyedited and formatted. The final version may differ from this version.

mutant channels harboring the homologous substitutions in hEAG1 (Y464A, F359L, L434C) were examined (Fig. 4*A* – *D*). Consistent with Leu434 contributing to ICA binding, L434C hEAG1 was less inhibited by ICA (IC_{50} = 4.8 ± 0.2 μM) compared to WT channels (Fig. 4*A* and *D*). As we reported previously, Y464A promotes and ICA accentuates prominent inactivation from an open state (Fig. 4*B* and *D*), whereas F359L (Fig. 4*C*) appears to promote and ICA reverses inactivation from closed states (Garg et al., 2012). Molecular modeling predicts that the F557L mutation in hERG1 excludes ICA from interaction with its hydrophobic binding pocket (Garg et al., 2011), consistent with its insensitivity to the drug. In contrast, molecular modeling predicts that the hydrophobic pocket in F359L hEAG1 channels can accommodate ICA (Supplemental Fig. 5), albeit in a different orientation as compared to the WT hEAG1 channel. Together, molecular modeling predictions and functional analysis of many mutant channels indicate that ICA modulates inactivation gating of both hEAG1 and hERG1channels by interacting with the same hydrophobic pocket defined by the S5-pore helix-S6 region of one subunit and S6 of an adjacent subunit. We next sought to determine if the functional effect of ICA could be reversed (i.e., switched from inhibitor to agonist) if the putative hydrophobic pocket of hEAG1 was modified by mutagenesis to mimic the pocket present in hERG1 channels.

Introducing Putative hERG1 Binding Pockets into hEAG1 Does Not Alter Response to ICA. The S5-pore helix-S6 regions of hERG1 and hEAG1 are composed of 79 residues and protein sequence alignment (Fig. 5*A*) indicates several differences between the two channels, including 8 residues in S5, 5 residues in the pore helix and 14 residues in S6. However, within the putative ICA binding pocket defined by docking simulations using the open state models of hERG1 (Garg et al., 2011) and hEAG1 (Fig. 3), only one residue in the pore helix and two residues in S6 differ between the two channels (Fig. 5*A*, highlighted in red text). Three amino

Downloaded from molpharm.aspetjournals.org at ASPET Journals on April 17, 2024

Molecular Pharmacology Fast Forward. Published on January 14, 2013 as DOI: 10.1124/mol.112.084384
This article has not been copyedited and formatted. The final version may differ from this version.

acid substitutions were introduced into hEAG1 (M431F in the pore helix; M458L and L463M in S6) to match the corresponding residues in hERG1. The resulting triple mutant (M431F/M458L/L463M) channel retained WT hEAG1 biophysical properties and response to ICA (Fig. 5*B*), including a similar IC_{50} value for inhibition of I_{end} (0.49 ± 0.15 μM, n = 3; Fig. 5*C*). Can the putative ICA binding site in hERG1 be adequately recapitulated in hEAG1 by just three amino acid substitutions? Molecular modeling suggests remarkable similar binding modes of the triple hEAG1 channel compared to the WT hERG1 channel. Simulated docking predicts that ICA binds perpendicular to the axis of the S5 and S6 segments in both the closed and open state and the nitro group faces towards the pore (Fig. 6), similar to the orientation of ICA in hERG1 (Garg et al., 2011). Furthermore, mutations M431F/M458L/L463M render the shape of the binding site more hERG1 like, allowing the drug to protrude deeply into the cleft formed by the interface of two adjacent subunits. Together these modeling and experimental findings support the notion that intrinsic differences in the mechanisms of slow versus fast inactivation gating, and not differences in the binding site, determines whether ICA is a channel antagonist (hEAG1) or agonist (hERG1).

Downloaded from molpharm.aspetjournals.org at ASPET Journals on April 17, 2024

Discussion

ICA Binds to a Common Site of EAG1 and ERG1 Channels to Exert Opposite Effects on Inactivation.

ICA inhibits outward K^+ hEAG1 channel currents by enhancing slow inactivation; i.e., it is an agonist of intrinsic slow inactivation gating. In contrast, ICA enhances outward hERG1 K^+ channel currents by antagonizing inactivation; i.e., it is an antagonist of intrinsic fast inactivation gating. Despite the opposite functional response to ICA, analysis of chimera ERG/EAG channels and multiple mutant channels clearly establish that the compound

Molecular Pharmacology Fast Forward. Published on January 14, 2013 as DOI: 10.1124/mol.112.084384
This article has not been copyedited and formatted. The final version may differ from this version.

binds to a similar region, in a hydrophobic cleft between two adjacent subunits of the pore module in both hERG1 and hEAG1. A recent molecular dynamics simulation study of hERG1 proposed that the binding pocket for ICA is located between the pore helices of two adjacent subunits and that the selectivity filter adopts a collapsed conformation in the inactivated state, precluding entry of the compound into the pocket. However, this binding mode does not include interaction with residues in S5, including F557, a residue that we find to be of particular importance in modification of channel gating by ICA (Kopfer et al., 2012). Given that both channels are homotetramers, there could be four identical ICA binding sites on each channel. Consistent with multiple binding sites, activation of hERG1 channels by ICA exhibits strong cooperativity, with a Hill coefficient of 3.3 estimated for the concentration-response relationship (Gerlach et al., 2010).

Slow inactivation of hEAG1 channels is modulated by a proposed interaction between three residues in close proximity and located in the S5 (Phe359), pore helix (Leu434) and S6 (Tyr464) of each subunit (Garg et al., 2012). In WT channels, inactivation is very slow and barely detectable, but is greatly enhanced by ICA or mutations of Tyr464. Y464A hEAG1 channels exhibit far greater intrinsic slow inactivation than WT channels and ICA accentuates this altered mode of gating. Inactivation of Y464A channels can be prevented (WT gating restored) by introducing a second mutation of either Leu434 or Phe359 (Garg et al., 2012). In contrast to Tyr464, multiple mutations of Leu434 or Phe359 do not alter the biophysical properties of hEAG1 (Garg et al., 2012), but do affect the response to ICA. F359A and L434A/C reduce the efficacy of ICA to induce inactivation, whereas highly inactivated F359L channels are activated by ICA. Together these findings suggest that ICA directly affects the molecular machinery of slow inactivation in hEAG1 channels.

Downloaded from molpharm.aspetjournals.org at ASPET Journals on April 17, 2024

Molecular Pharmacology Fast Forward. Published on January 14, 2013 as DOI: 10.1124/mol.112.084384
This article has not been copyedited and formatted. The final version may differ from this version.

F359A and F359L hEAG1 channels exhibited altered responses to ICA. F359A channels were less sensitive to inhibition by ICA (67-fold increase in IC_{50}), indicating a reduced binding affinity. In addition, ICA reduced F359A channel currents without inducing the prominent time-dependent decay of current during depolarizing pulse seen with WT channels. We interpret this later effect to indicate that ICA enhances closed (but not open) state inactivation of F359A channels. Inhibition of F359A channels could also result from open channel block; however, we have previously presented extensive evidence that ICA induces both closed and open state inactivation of WT hEAG1 channels with no evidence of open channel block (Garg et al., 2012). Based on our molecular modeling results, ICA binds similarly to the open state of WT and F359L hEAG1 channels [compare Supplemental Fig 2D, E (WT) and Supplemental Fig 5A, B (F359L)]. However, unlike WT channels, the activation of F359L channels was biphasic: currents were activated at all concentrations examined (1-30 μM) and peaked at 3 μM. ICA concentrations > 3 μM led to progressively less activation that was accompanied by progressively more extensive time-dependent decay of outward currents (indicative of enhanced open channel inactivation). Based on injection of oocytes with equivalent amounts of cRNA, F359L hEAG1 channel currents are much smaller than WT channel current, suggesting that these mutant channels are either highly inactivated or have a lower than normal single channel open probability. As discussed previously (Garg et al., 2012), we propose that ICA mediated increase of F359L channel currents may be caused by a reduced rate of closed to inactivated state transitions.

Modification of channel gating has also been proposed as the mechanism responsible for activation of KCNQ2-5 (Kv7.2-Kv7.5) channels by retigabine, an anticonvulsant drug that shifts the voltage dependence of activation to more negative potentials. The putative binding site for

Downloaded from molpharm.aspetjournals.org at ASPET Journals on April 17, 2024

Molecular Pharmacology Fast Forward. Published on January 14, 2013 as DOI: 10.1124/mol.112.084384
This article has not been copyedited and formatted. The final version may differ from this version.

retigabine is a hydrophobic binding pocket (Lange et al., 2009; Schenzer et al., 2005; Wuttke et al., 2005) located in the same region described here for ICA binding to ERG and EAG channels. The primary molecular determinants of retigabine binding in KCNQ3 are Trp265 (S5), Leu314 (pore helix) and Leu338 (S6), homologous to key components of the ICA binding site in hEAG1 (Phe359, Leu434, Met458) and hERG1 (Phe557, Leu622, Leu646). Moreover, mutation of the aromatic residue in S5 to Leu renders hERG (F557L) channels insensitive to ICA and KCNQ3 (W265L) channels insensitive to retigabine. The homologous mutation in hEAG1 (F359L) reversed the effect of ICA from antagonist to agonist activity, while the reverse mutation at the corresponding residue in KCNQ1 (L266W) leads to inhibition in a channel that is normally insensitive to retigabine (Schenzer et al., 2005). Another interesting analogy between EAG and KCNQ (specifically, KCNQ1) channels is that in both, a tripartite mode of inactivation gating has been proposed, involving specific residues in the S5, pore helix and S6 (Seebohm et al., 2005). Thus, gating of the selectivity filter in multiple, unrelated Kv channels is modulated by binding of lipophilic compounds to the hydrophobic cleft situated between two adjacent subunits in the pore module.

Clinical relevance. Treatments for congenital and acquired long QT syndrome (LQTS) are limited. The recent discovery of several compounds that activate hERG1 channels initiates a promising pathway towards discovery and development of genotype specific therapy for this life-threatening disorder. As a consequence of its profound inhibition of inactivation, ICA increases the magnitude of outward hERG1 currents far more than has been observed for other activators such as RPR260243 (Kang et al., 2005), PD-118057 (Perry et al., 2007) or NS1643 (Grunnet et al., 2010; Hansen et al., 2006). A hERG1 activator that has more modest effect on current magnitude than ICA would be less prone to induce excessive shortening of action potentials and

Downloaded from molpharm.aspetjournals.org at ASPET Journals on April 17, 2024

Molecular Pharmacology Fast Forward. Published on January 14, 2013 as DOI: 10.1124/mol.112.084384
This article has not been copyedited and formatted. The final version may differ from this version.

avoid the potential conversion of long to short QT syndrome. In addition, our findings warn that hERG1 agonists may also affect the gating of highly related hEAG1 channels with potential functional consequences in the CNS.

Downloaded from molpharm.aspetjournals.org at ASPET Journals on April 17, 2024

Molecular Pharmacology Fast Forward. Published on January 14, 2013 as DOI: 10.1124/mol.112.084384
This article has not been copyedited and formatted. The final version may differ from this version.

Acknowledgments

We thank Alison Gardner and Jennifer Abbruzzese for technical assistance. The computational results were achieved using the Vienna Scientific Cluster (VSC).

Downloaded from molpharm.aspetjournals.org at ASPET Journals on April 17, 2024

Molecular Pharmacology Fast Forward. Published on January 14, 2013 as DOI: 10.1124/mol.112.084384
This article has not been copyedited and formatted. The final version may differ from this version.

Authorship Contributions:

Participated in research design: Garg, Stary-Weinzinger, Sanguinetti

Conducted experiments: Garg

Performed data analysis: Garg, Stary-Weinzinger, Sanguinetti

Wrote or contributed to the writing of the manuscript: Garg, Stary-Weinzinger, Sanguinetti

Downloaded from molpharm.aspetjournals.org at ASPET Journals on April 17, 2024

Molecular Pharmacology Fast Forward. Published on January 14, 2013 as DOI: 10.1124/mol.112.084384
This article has not been copyedited and formatted. The final version may differ from this version.

References

Chen J, Avdonin V, Ciorba MA, Heinemann SH and Hoshi T (2000) Acceleration of P/C-type inactivation in voltage-gated K^+ channels by methionine oxidation. *Biophys J* **78**:174-187.

Darden T, York D and Pedersen L (1993) Particle mesh Ewald: An *N*-log(*N*) method for Ewald sums in large systems. *J Chem Phys* **98**:10089-10092.

Doyle DA, Morais Cabral J, Pfuetzner RA, Kuo A, Gulbis JM, Cohen SL, Chait BT and MacKinnon R (1998) The structure of the potassium channel: molecular basis of K^+ conduction and selectivity. *Science* **280**:69-77.

Ficker E, Jarolimek W, Kiehn J, Baumann A and Brown AM (1998) Molecular determinants of dofetilide block of HERG K^+ channels. *Circ Res* **82**:386-395.

Frisch MJ, Trucks GW, Schlegel HB, Scuseria GE, Robb MA, Cheeseman JR and Scalmani G (2009) *Gaussian 09, Revision A.1* Gaussian, Inc., Wallingford.

Garg V, Sachse FB and Sanguinetti MC (2012) Tuning of EAG K^+ channel inactivation: Molecular determinants of amplification by mutations and a small molecule. *J Gen Physiol* **140**:307-324.

Garg V, Stary-Weinzinger A, Sachse F and Sanguinetti MC (2011) Molecular determinants for activation of human ether-a-go-go-related gene 1 potassium channels by 3-nitro-N-(4-phenoxyphenyl) benzamide. *Mol Pharmacol* **80**:630-637.

Gerlach AC, Stoehr SJ and Castle NA (2010) Pharmacological removal of human ether-a-go-go-related gene potassium channel inactivation by 3-nitro-N-(4-phenoxyphenyl) benzamide (ICA-105574). *Mol Pharmacol* **77**:58-68.

Downloaded from molpharm.aspetjournals.org at ASPET Journals on April 17, 2024

Molecular Pharmacology Fast Forward. Published on January 14, 2013 as DOI: 10.1124/mol.112.084384
This article has not been copyedited and formatted. The final version may differ from this version.

Goldin AL (1991) Expression of ion channels by injection of mRNA into *Xenopus* oocytes. *Methods Cell Biol* **36**:487-509.

Grunnet M, Abbruzzese J, Sachse FB and Sanguinetti MC (2010) Molecular determinants of hERG1 K^+ channel activation by NS1643. *Mol Pharmacol* **79**:1-9.

Hansen RS, Diness TG, Christ T, Demnitz J, Ravens U, Olesen SP and Grunnet M (2006) Activation of human ether-a-go-go-related gene potassium channels by the diphenylurea 1,3-bis-(2-hydroxy-5-trifluoromethyl-phenyl)-urea (NS1643). *Mol Pharmacol* **69**:266-277.

Hemmerlein B, Weseloh RM, Mello de Queiroz F, Knotgen H, Sanchez A, Rubio ME, Martin S, Schliephacke T, Jenke M, Heinz Joachim R, Stuhmer W and Pardo LA (2006) Overexpression of Eag1 potassium channels in clinical tumours. *Mol Cancer* **5**:41.

Hess B, Bekker H, Berendsen HJC and Fraaije JGEM (1997) LINCS: A linear constraint solver for molecular simulations. *J Comp Chem* **18**:1463-1472.

Hess B, Kutzner C, van der Spoel D and Lindahl E (2008) GROMACS 4: Algorithms for highly efficient, load-balanced, and scalable molecular simulation. *J Chem Theory Comput* **4**:435–447.

Hornak V, Abel R, Okur A, Strockbine B, Roitberg A and Simmerling C (2006) Comparison of multiple Amber force fields and development of improved protein backbone parameters. *Proteins* **65**:712-725.

Hoshi T, Zagotta WN and Aldrich RW (1990) Biophysical and molecular mechanisms of *Shake*r potassium channel inactivation. *Science* **250**:533-538.

Hoshi T, Zagotta WN and Aldrich RW (1991) Two types of inactivation in *Shaker* K^+ channels: effects of alterations in the carboxy-terminal region. *Neuron* **7**:547-556.

Downloaded from molpharm.aspetjournals.org at ASPET Journals on April 17, 2024

Molecular Pharmacology Fast Forward. Published on January 14, 2013 as DOI: 10.1124/mol.112.084384
This article has not been copyedited and formatted. The final version may differ from this version.

Jiang Y, Lee A, Chen J, Ruta V, Cadene M, Chait BT and MacKinnon R (2003) X-ray structure of a voltage-dependent K^+ channel. *Nature* **423**:33-41.

Jones G, Willett P and Glen RC (1995) Molecular recognition of receptor sites using a genetic algorithm with a description of desolvation. *J Mol Biol* **245**:43-53.

Jorgensen WL, Chandrasekhar J, Madura JD, Impey RW and M.L. K (1983) Comparison of simple potential functions for simulating liquid water. *J Chem Phys* **79**:926-935.

Kang J, Chen XL, Wang H, Ji J, Cheng H, Incardona J, Reynolds W, Viviani F, Tabart M and Rampe D (2005) Discovery of a small molecule activator of the Human Ether-a-go-go-Related Gene (HERG) cardiac K^+ channel. *Mol Pharmacol* **67**:827-836.

Knape K, Linder T, Wolschann P, Beyer A and Stary-Weinzinger A (2011) In silico analysis of conformational changes induced by mutation of aromatic binding residues: consequences for drug binding in the hERG K^+ channel. *PLoS One* **6**:e28778.

Kopfer DA, Hahn U, Ohmert I, Vriend G, Pongs O, de Groot BL and Zachariae U (2012) A molecular switch driving inactivation in the cardiac K^+ channel HERG. *PLoS One* **7**:e41023.

Lange W, Geissendorfer J, Schenzer A, Grotzinger J, Seebohm G, Friedrich T and Schwake M (2009) Refinement of the binding site and mode of action of the anticonvulsant Retigabine on KCNQ K^+ channels. *Mol Pharmacol* **75**:272-280.

Ludwig J, Terlau H, Wunder F, Bruggemann A, Pardo LA, Marquardt A, Stuhmer W and Pongs O (1994) Functional expression of a rat homologue of the voltage gated either a go-go potassium channel reveals differences in selectivity and activation kinetics between the Drosophila channel and its mammalian counterpart. *EMBO J* **13**:4451-4458.

Downloaded from molpharm.aspetjournals.org at ASPET Journals on April 17, 2024

Molecular Pharmacology Fast Forward. Published on January 14, 2013 as DOI: 10.1124/mol.112.084384
This article has not been copyedited and formatted. The final version may differ from this version.

Martin S, Lino de Oliveira C, Mello de Queiroz F, Pardo LA, Stuhmer W and Del Bel E (2008) Eag1 potassium channel immunohistochemistry in the CNS of adult rat and selected regions of human brain. *Neuroscience* **155**:833-844.

Mello de Queiroz F, Suarez-Kurtz G, Stuhmer W and Pardo LA (2006) Ether a go-go potassium channel expression in soft tissue sarcoma patients. *Mol Cancer* **5**:42.

Nose S (1984) A unified formulation of the constant temperature molecular dynamics methods. *J Chem Phys* **81(1)**:511-519.

Pardo LA, del Camino D, Sanchez A, Alves F, Bruggemann A, Beckh S and Stühmer W (1999) Oncogenic potential of EAG K^+ channels. *EMBO J* **18**:5540-5547.

Parrinello M and Rahman A (1981) Polymorphic transitions in single crystals: A new molecular dynamics method. *J Applied Phys* **52**:7182-7190.

Perry M, Sachse FB and Sanguinetti MC (2007) Structural basis of action for a human ether-a-go-go-related gene 1 potassium channel activator. *Proc Natl Acad Sci USA* **104**:13827–13832.

Sanguinetti MC, Jiang C, Curran ME and Keating MT (1995) A mechanistic link between an inherited and an acquired cardiac arrhythmia: *HERG* encodes the I_{Kr} potassium channel. *Cell* **81**:299-307.

Sanguinetti MC and Jurkiewicz NK (1990) Two components of cardiac delayed rectifier K^+ current: Differential sensitivity to block by class III antiarrhythmic agents. *J Gen Physiol* **96**:195-215.

Sanguinetti MC and Tristani-Firouzi M (2006) hERG potassium channels and cardiac arrhythmia. *Nature* **440**:463-469.

Downloaded from molpharm.aspetjournals.org at ASPET Journals on April 17, 2024

Molecular Pharmacology Fast Forward. Published on January 14, 2013 as DOI: 10.1124/mol.112.084384
This article has not been copyedited and formatted. The final version may differ from this version.

Schenzer A, Friedrich T, Pusch M, Saftig P, Jentsch TJ, Grotzinger J and Schwake M (2005) Molecular determinants of KCNQ (Kv7) K^+ channel sensitivity to the anticonvulsant retigabine. *J Neurosci* **25**:5051-5060.

Schreibmayer W, Lester HA and Dascal N (1994) Voltage clamping of *Xenopus laevis* oocytes utilizing agarose-cushion electrodes. *Pflugers Arch* **426**:453-458.

Seebohm G, Westenskow P, Lang F and Sanguinetti MC (2005) Mutation of colocalized residues of the pore helix and transmembrane segments S5 and S6 disrupt deactivation and modify inactivation of KCNQ1 K^+ channels. *J Physiol* **563**:359-368.

Siu SW, Vacha R, Jungwirth P and Bockmann RA (2008) Biomolecular simulations of membranes: physical properties from different force fields. *J Chem Phys* **128**:125103.

Smith PL, Baukrowitz T and Yellen G (1996) The inward rectification mechanism of the HERG cardiac potassium channel. *Nature* **379**:833-836.

Spector PS, Curran ME, Zou A, Keating MT and Sanguinetti MC (1996) Fast inactivation causes rectification of the I_{Kr} channel. *J Gen Physiol* **107**:611-619.

Stansfeld PJ, Grottesi A, Sands ZA, Sansom MS, Gedeck P, Gosling M, Cox B, Stanfield PR, Mitcheson JS and Sutcliffe MJ (2008) Insight into the mechanism of inactivation and pH sensitivity in potassium channels from molecular dynamics simulations. *Biochemistry* **47**:7414-7422.

Stary A, Wacker SJ, Boukharta L, Zachariae U, Karimi-Nejad Y, Aqvist J, Vriend G and de Groot BL (2010) Toward a consensus model of the HERG potassium channel. *ChemMedChem* **5**:455-467.

Stühmer W (1992) Electrophysiological recording from *Xenopus* oocytes. *Methods Enzymol* **207**:319-339.

Downloaded from molpharm.aspetjournals.org at ASPET Journals on April 17, 2024

Molecular Pharmacology Fast Forward. Published on January 14, 2013 as DOI: 10.1124/mol.112.084384
This article has not been copyedited and formatted. The final version may differ from this version.

Suessbrich H, Schonherr R, Heinemann SH, Lang F and Busch AE (1997) Specific block of cloned Herg channels by clofilium and its tertiary analog LY97241. *FEBS Lett* **414**:435-438.

Trudeau M, Warmke JW, Ganetzky B and Robertson GA (1995) HERG, A human inward rectifier in the voltage-gated potassium channel family. *Science* **269**:92-95.

Warmke J, Drysdale R and Ganetzky B (1991) A distinct potassium channel polypeptide encoded by the *Drosophila eag* locus. *Science* **252**:1560-1564.

Warmke JW and Ganetzky B (1994) A family of potassium channel genes related to *eag* in *Drosophila* and mammals. *Proc Natl Acad Sci USA* **91**:3438-3442.

Wuttke TV, Seebohm G, Bail S, Maljevic S and Lerche H (2005) The new anticonvulsant retigabine favors voltage-dependent opening of the Kv7.2 (KCNQ2) channel by binding to its activation gate. *Mol Pharmacol* **67**:1009-1017.

Ye S, Li Y and Jiang Y (2003) Novel insights into K^+ selectivity from high-resolution structures of an open K^+ channel pore. *Nat Struct Mol Biol* **17**:1019-1023.

Zhang H, Zou B, Yu H, Moretti A, Wang X, Yan W, Babcock JJ, Bellin M, McManus OB, Tomaselli G, Nan F, Laugwitz KL and Li M (2012) Modulation of hERG potassium channel gating normalizes action potential duration prolonged by dysfunctional KCNQ1 potassium channel. *Proc Natl Acad Sci USA* **109**:11866-11871.

Downloaded from molpharm.aspetjournals.org at ASPET Journals on April 17, 2024

Molecular Pharmacology Fast Forward. Published on January 14, 2013 as DOI: 10.1124/mol.112.084384
This article has not been copyedited and formatted. The final version may differ from this version.

Footnotes:

This work was supported by National Institutes of Health/National Heart, Lung, and Blood Institute [Grant HL055236] to M.S., an American Heart Association (Western States Affiliate) postdoctoral fellowship to V.G., and The Austrian Science Fund [Grant P22395] to A. S-W.

Reprint requests: M.C. Sanguinetti, Nora Eccles Harrison Cardiovascular Research & Training Institute, Department of Physiology and Medicine, University of Utah, 95 South 2000 East, Salt Lake City, UT 84112; E-mail: sanguinetti@cvrti.utah.edu

Downloaded from molpharm.aspetjournals.org at ASPET Journals on April 17, 2024

Molecular Pharmacology Fast Forward. Published on January 14, 2013 as DOI: 10.1124/mol.112.084384
This article has not been copyedited and formatted. The final version may differ from this version.

Figure legends

Fig. 1. The pore domain of EAG1 and ERG1 channels determines functional response to ICA. *(A*) ICA activates WT hERG1 channel current. (*B*) ICA inhibits WT hEAG1 channel current. For traces shown in panels A and B, currents were activated with 10-s pulses to +30 mV from a holding potential of -100 mV. (*C*) [ICA]-response relationship for inhibition of hEAG1 channel currents (n = 5). ICA inhibited I_{end}, current at the end of a 10-s pulse to +30 mV (IC_{50} = 0.44 ± 0.03 μM; n_H = 2.3) more potently than I_{peak}, peak outward current (IC_{50} = 1.38 ± 0.04 μM; n_H = 1.4). *D – I:* Effect of ICA on EAG1/ERG1 chimera channels. In each panel, the diagram indicates regions of subunits contributed by bEAG1 (black) and hERG1 (gray). Currents were elicited with 10-s pulses to +30 mV from a holding potential of -100 mV. The fold-change in I_{end} induced by ICA, for each chimera channels was as follows: (*D*) EAG/$ERG_{S45L-S6}$ (1.9 ± 0.03 at 10 μM; 3.6 ± 0.6 at 30 μM, n = 3). (*E*) ERG/$EAG_{S45L-S6}$ (0.58 ± 0.07 at 1 μM; 0.24 ± 0.04 at 3 μM, n = 4). (*F*) ERG/EAG_{S6} (9.6 ± 3.5 at 10 μM; 41 ± 11 at 30 μM, n = 4). (*G*) ERG/EAG_{turret} (15 ± 1.9 at 10 μM; 26 ± 0.3 at 30 μM, n = 3). (*H*) ERG/$EAG_{S45L-S5}$ (9.7 ± 1.6 at 10 μM; 6.1 ± 1.0 at 30 μM, n = 3). (*I*) ERG/$EAG_{turret\text{-}pore\ helix\text{-}selectivity\ filter}$ (% change in I_{end}: 9 ± 3 at 3 μM; 4 ± 2 at 10 μM; -3 ± 3 at 30 μM, n = 3).

Fig. 2. ICA has dual effects on fast-inactivating T432S/A443S hEAG1 channels.
(A) Representative traces illustrating the effect of 3 and 30 μM ICA on current measured at a test potential of +30 mV. Currents were elicited from a holding potential of −60 mV. (*B and C*) Normalized I_{peak}-V relationships (*B*) and I_{end}-V (*C*) relationships measured before (Control) and in the presence of indicated [ICA] (n = 5). (*D)* [ICA]-response relationships for I_{peak} (solid curve) and I_{end} (dashed curve) measured at a single (+30 mV) test potential for T432S/A443S (data

Downloaded from molpharm.aspetjournals.org at ASPET Journals on April 17, 2024

Molecular Pharmacology Fast Forward. Published on January 14, 2013 as DOI: 10.1124/mol.112.084384
This article has not been copyedited and formatted. The final version may differ from this version.

points, ■ and ○) and WT hEAG1. The IC_{50} for I_{peak} was 7.6 ± 0.9 μM for T432S/A443S hEAG1 (n = 5).

Fig. 3. Models of ICA docked to the open and closed state of the hEAG1 pore module. (*A)* Single ICA molecule (shown in space-fill) docked to the open state model of the complete pore module as viewed from the extracellular space. (*B)* Side view of the S5-S6 regions of two adjacent hEAG1 subunits of an open state channel. ICA molecule is shown in transparent space-fill; interacting residues are shown as green sticks. (*C)* Close-up view of panel B with interacting residues labeled. (*D – F)* ICA bound to the closed state model of the hERG1 pore module.

Fig. 4. Concentration-dependent effects of ICA on L434C, Y464A and F359L hEAG1 channels. (*A)* Effect of ICA (1 μM – 30 μM) on L434C hEAG1 channel currents measured in response to 10-s depolarization to +30 mV. (*B)* Effect of ICA (25 nM – 1 μM) on Y464A hEAG1 channel currents during 10-s pulse to +30 mV. (*C*) Biphasic response of F359L hEAG1 channels to ICA (1 μM – 30 μM) during 10-s pulse to +30 mV. (*D)* [ICA]-response (normalized I_{end}) relationships for indicated WT and mutant hEAG1 channels. The IC_{50} for I_{end} was 0.07 ± 0.01 μM for Y464A (n = 3), 4.8 ± 0.2 μM for L434C (n = 3) and >30 μM for F359L (n = 4) hEAG1 channels. WT data is same as that plotted in Fig. 1*C*.

Fig. 5. ICA-induces inactivation of mutant hEAG1 channel with putative drug binding pocket engineered to mimic hERG1 channel. (*A*) Amino acid sequence alignment of S5 and pore helix (PH)/selectivity filter (SF)/S6 region of hEAG1 and hERG1. Non-conserved amino acids are underlined. Conserved residues (blue) and non-conserved residues (red) predicted to line the

Downloaded from molpharm.aspetjournals.org at ASPET Journals on April 17, 2024

Molecular Pharmacology Fast Forward. Published on January 14, 2013 as DOI: 10.1124/mol.112.084384
This article has not been copyedited and formatted. The final version may differ from this version.

hydrophobic ICA binding pocket in hERG1 are highlighted. Residues colored green were predicted to contribute to ICA binding site in closed state of hEAG1 (but not predicted to interact with hERG1 in closed or open state). (*B*) Concentration-dependent inhibition of M431F/M458L/L463M hEAG1 channel currents by ICA. Currents were elicited with 10-s pulses to +30 mV. **(***C*) [ICA]-response relationships for I_{peak} (solid curve) and I_{end} (dashed curve) quantified as fold change in current measured at a test potential of +30 mV for M431F/M458L/L463M (data points, ■ and ○) and WT hEAG1 (curves only, replotted from Fig. 1*C*). The IC_{50} was 0.49 ± 0.15 μM for I_{end} and 2.96 ± 0.82 μM for I_{peak} (n = 4).

Fig. 6. Molecular models of ICA docked to M431F/M458L/L463M hEAG1 channel pore module. (*A* and *B*) Open state model. (*C* and *D*) Closed state model.

Downloaded from molpharm.aspetjournals.org at ASPET Journals on April 17, 2024

Molecular Pharmacology Fast Forward. Published on January 14, 2013 as DOI: 10.1124/mol.112.084384
This article has not been copyedited and formatted. The final version may differ from this version.

Table 1. Mutant hEAG1 channels with altered response to ICA.

Mutation in hEAG1	**IC_{50} for ICA (μM)** **Avg.**	**s.e.m.**	***n***	**Fold increase or decrease (↓) in IC_{50}**
(WT)	0.44	0.03	5	--
V356A**	0.08	0.009	3	5.5 ↓
*V356E***	28.8	2.6	3	65
F359A*	29.6	9.0	3	67
F359L	>30	--	4	>68
L427A**	0.17	0.01	3	2.6 ↓
M431A*	1.9	0.34	5	4.3
L434A**	8.5	0.08	5	19
*L434C***	4.8	0.2	3	11
M457A	>30	--	4	>68
M458A**	20.2	1.2	4	46[#]
M458E[¶]	0.45	0.08	3	no change
L462A**	0.05	0.005	3	8.6 ↓
L463A**	41.2	8.2	3	94[#]
Y464A**	0.07	0.014	3	6.3 ↓
I467A**	1.1	0.05	3	2.5
*I467E***	24.8	4.1	3	56[#]
F468A**	3.1	0.48	4	7

[¶]NS: non-significant ($p > 0.05$); *$p < 0.01$, **$p < 0.001$ compared to WT; [#]effective IC_{50}

Downloaded from molpharm.aspetjournals.org at ASPET Journals on April 17, 2024

Figure 1

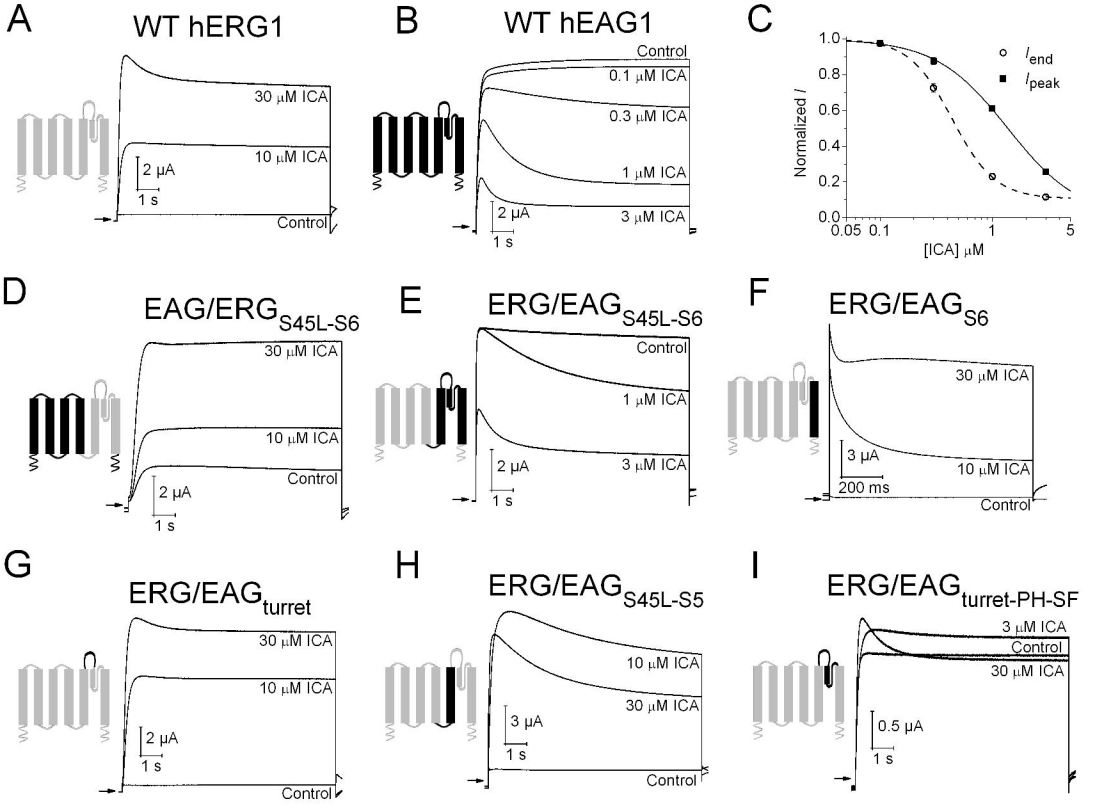
A
WT hERG1
30 μM ICA
10 μM ICA
2 μA
1 s
Control
B
WT hEAG1
Control
0.1 μM ICA
0.3 μM ICA
1 μM ICA
3 μM ICA
2 μA
1 s
C
Normalized I
1.0
0.8
0.6
0.4
0.2
0.0
0.05 0.1
1
5
[ICA] μM
I end
I peak
D
EAG/ERG S45L-S6
30 μM ICA
10 μM ICA
Control
2 μA
1 s
E
ERG/EAG S45L-S6
Control
1 μM ICA
3 μM ICA
2 μA
1 s
F
ERG/EAG S6
30 μM ICA
3 μA
10 μM ICA
200 ms
Control
G
ERG/EAG turret
30 μM ICA
10 μM ICA
2 μA
1 s
Control
H
ERG/EAG S45L-S5
10 μM ICA
30 μM ICA
3 μA
1 s
Control
I
ERG/EAG turret-PH-SF
3 μM ICA
Control
30 μM ICA
0.5 μA
1 s

Figure 2

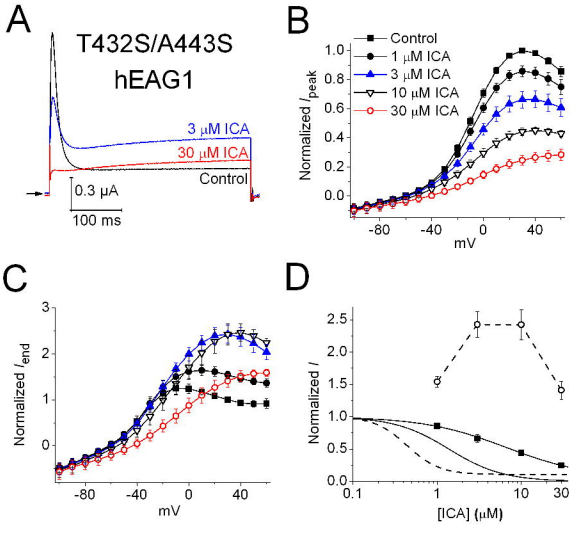
A
T432S/A443S
hEAG1
3 μM ICA
30 μM ICA
Control
0.3 μA
100 ms
B
Control
1 μM ICA
3 μM ICA
10 μM ICA
30 μM ICA
Normalized I_{peak}
mV
C
Normalized I_{end}
mV
D
Normalized I
[ICA] (μM)

Molecular Pharmacology Fast Forward. Published on January 14, 2013 as DOI: 10.1124/mol.112.084384
This article has not been copyedited and formatted. The final version may differ from this version.

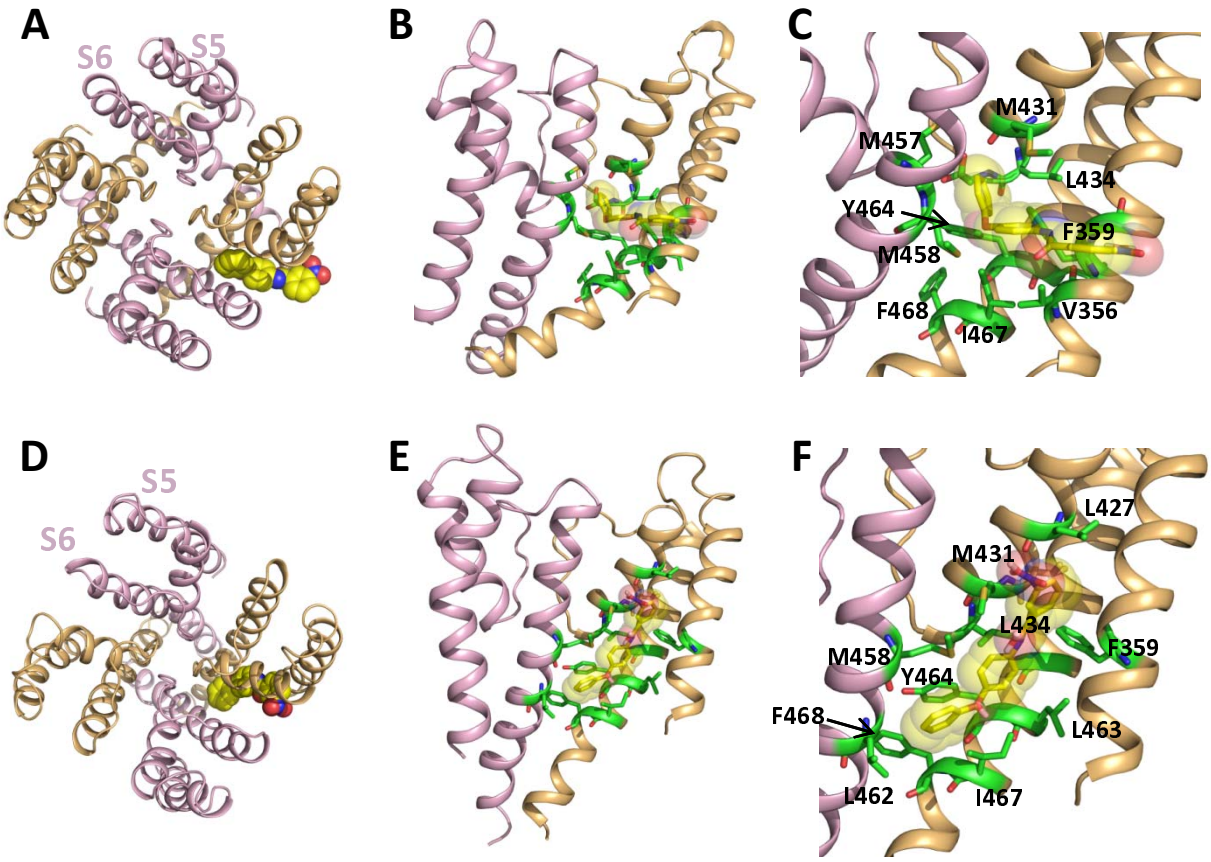

Figure 3

Downloaded from molpharm.aspetjournals.org at ASPET Journals on April 17, 2024

Figure 4

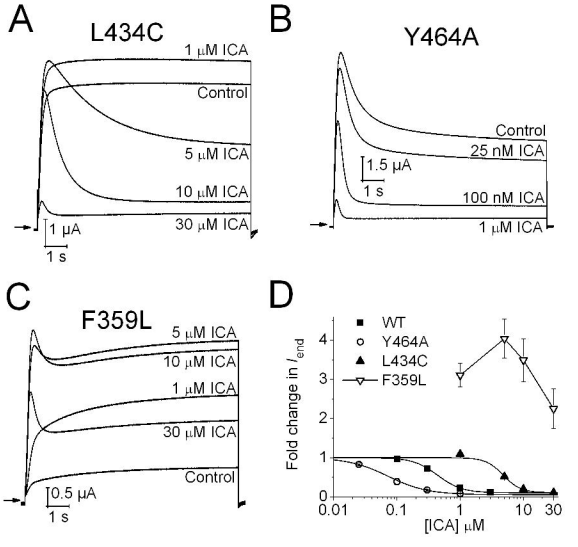
A
L434C
1 μM ICA
Control
5 μM ICA
10 μM ICA
30 μM ICA
1 μA
1 s
B
Y464A
Control
25 nM ICA
1.5 μA
1 s
100 nM ICA
1 μM ICA
C
F359L
5 μM ICA
10 μM ICA
1 μM ICA
30 μM ICA
Control
0.5 μA
1 s
D
WT
Y464A
L434C
F359L
Fold change in I_{end}
0
1
2
3
4
0.01
0.1
1
10
30
[ICA] μM

Figure 5

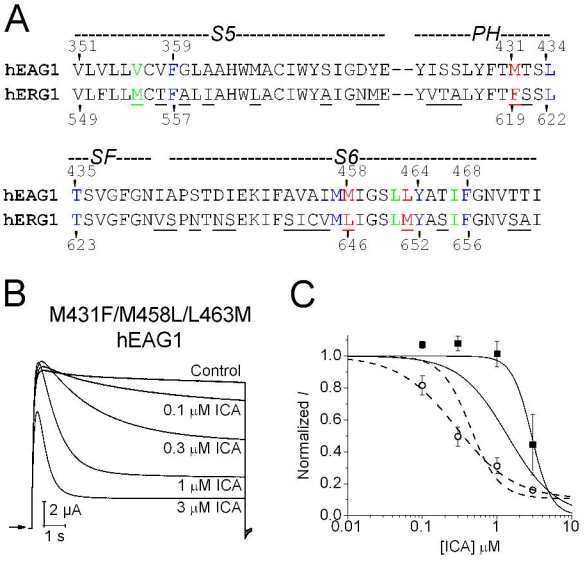
A
S5
PH
hEAG1 VLVLLVCVFGLAAHWMACIWYSIGDYE--YISSLYFTMTSL
hERG1 VLFLLMCTFALIAHWLACIWYAIGNME--YVTALYFTFSSL
SF
S6
hEAG1 TSVGFGNIAPSTDIEKIFAVAIMMIGSLLYATIFGNVTTI
hERG1 TSVGFGNVSPNTNSEKIFSICVMLIGSLMYASIFGNVSAI
B
M431F/M458L/L463M
hEAG1
Control
0.1 μM ICA
0.3 μM ICA
1 μM ICA
3 μM ICA
2 μA
1 s
C
Normalized I
[ICA] μM

Molecular Pharmacology Fast Forward. Published on January 14, 2013 as DOI: 10.1124/mol.112.084384
This article has not been copyedited and formatted. The final version may differ from this version.

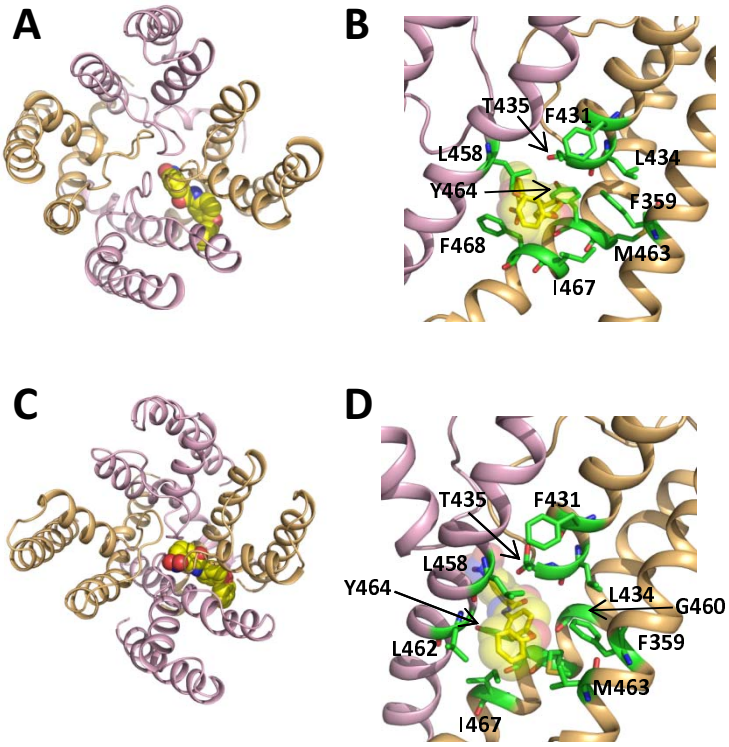

Figure 6

Downloaded from molpharm.aspetjournals.org at ASPET Journals on April 17, 2024